nanomanufacturing

MDPI

Article

Amphiphilic P(OEGMA-*co*-DIPAEMA) Hyperbranched Copolymer/Magnetic Nanoparticle Hybrid Nanostructures by Co-Assembly

Dimitrios Selianitis [1], Aleksander Forys [2], Barbara Trzebicka [2], Adam Alemayehu [3], Václav Tyrpekl [3] and Stergios Pispas [1,*]

[1] Theoretical and Physical Chemistry Institute, National Hellenic Research Foundation, 48 Vassileos Constantinou Avenue, 11635 Athens, Greece; dselianitis@eie.gr
[2] Centre of Polymer and Carbon Materials, Polish Academy of Sciences, 34 ul. M. Curie-Skłodowskiej, 41-819 Zabrze, Poland; aforys@cmpw-pan.edu.pl (A.F.); barbara.trzebicka@cmpw-pan.edu.pl (B.T.)
[3] Department of Inorganic Chemistry, Faculty of Science, Charles University in Prague, Albertov 6, 128-43 Praha 2, 11636 Prague, Czech Republic; adam.alemayehu@natur.cuni.cz (A.A.); vaclav.tyrpekl@natur.cuni.cz (V.T.)
* Correspondence: pispas@eie.gr; Tel.: +30-210-727-3824

Abstract: This work presents the utilization of amphiphilic poly(oligo(ethylene glycol) methyl methacrylate)-*co*-poly(2-(diisopropylamino)ethyl methacrylate), P(OEGMA-*co*-DIPAEMA), hyperbranched (HB) copolymers, forming polymeric aggregates in aqueous media, as building nanocomponents and nanocarriers for the entrapment of magnetic cobalt ferrite nanoparticles ($CoFe_2O_4$, MNPs), and the hydrophobic drug curcumin (CUR) in their hydrophobic domains. Dynamic light scattering (DLS) and cryogenic transmission electron microscopy (cryo-TEM) techniques were used to evaluate the multifunctional hybrid nanostructures formed in aqueous media by co-assembly of the components and their solution properties. Magnetic nanoparticles (MNPs) or MNPs/CUR were co-assembled effectively with pre-existing polymer aggregates, leading to well-defined hybrid nanostructures. Magnetophoresis experiments revealed that the hybrid nanostructures retain the magnetic properties of MNPs after their co-assembly with the hyperbranched copolymers. The hybrid nanostructures demonstrate a significant colloidal stability under physiological conditions. Furthermore, MNPs/CUR-loaded aggregates displayed considerable fluorescence as demonstrated by fluorescence spectroscopy. These hybrid nanostructures could be promising candidates for drug delivery and bio-imaging applications.

Keywords: hyperbranched copolymers; magnetic nanoparticles; curcumin; hybrid nanostructures; bio-imaging

Citation: Selianitis, D.; Forys, A.; Trzebicka, B.; Alemayehu, A.; Tyrpekl, V.; Pispas, S. Amphiphilic P(OEGMA-*co*-DIPAEMA) Hyperbranched Copolymer/Magnetic Nanoparticle Hybrid Nanostructures by Co-Assembly. *Nanomanufacturing* **2022**, 2, 53–68. https://doi.org/10.3390/nanomanufacturing2010004

Academic Editor: Donato Cosco

Received: 28 December 2021
Accepted: 7 February 2022
Published: 1 March 2022

1. Introduction

Polymeric materials that act as a drug used for imaging and therapeutic agents simultaneously have gained the interest of the scientific community in recent years. Therefore, they are being extensively developed and constructed due to their multi-functionality for the cure of various life-threatening diseases. A wide range of research has been reported to procure the effectiveness of such materials in theranostic applications [1–9]. Polymer nanomedicine is based on the development of copolymers that are biodegradable and biocompatible, and provides bioavailability and colloidal stability to the formed multifunctional hybrid nanomaterials and entrapped species.

Hyperbranched polymeric nanostructures have attracted the interest of polymer science as they present significantly different structural properties [10–13]. Hyperbranched polymers have many advantages in being used as nanocomponents for a wide range of biomedical applications, such as drug delivery and bio-imaging, due to their unique properties. More importantly they exhibit small sizes at the nanoscale, similar to dendrimers. Also,

they can be easily synthesized by one-step polymerization, which means they are economical products for large-scale industrial applications [14,15]. Amphiphilic hyperbranched copolymers are able to be self-assembled into various complex nanostructures when inserted in aqueous media, where the hydrophobic component forms hydrophobic domains and the hydrophilic component forms more solvated outer domains. Their self-organized structures/morphologies depend on the ratio of hydrophilic to hydrophobic segments. This property makes them potential nanomaterials for the entrapment and delivery of hydrophobic molecules/species, such as drugs [16,17] and imaging probes [18,19]. The entrapment of inorganic nanoparticles in the self-organized structures of hyperbranched copolymers leads to the formation of hybrid nanomaterials with increased colloidal stability, facile multi-functionalities and limited toxicity, with a combination of characteristics of both the nanoparticles and the copolymers [20,21]. Several research groups have developed MNPs/polymer hybrid nanostructures to investigate their properties in fields such as magnetic resonance imaging (MRI). In most cases the formed hybrid nanostructures show efficient stabilization of MNPs in aqueous solutions [19,22,23]. Other biomedical applications of MNPs/polymer hybrid nanoparticles include magnetic hyperthermia [24–26] and drug delivery [27–29] for effective, active, and triggered release [30,31] of the entrapped drugs. Another interesting application of hybrid nanostructures, is that they could be used to remove polycyclic hydrocarbon pollutants from aqueous media [32].

The present work focuses on the preparation of hybrid nanostructures by co-assembly of amphiphilic poly(oligo(ethylene glycol) methyl methacrylate)-*co*-poly(2-(diisopropylamino)ethyl methacrylate) P(OEGMA-*co*-DIPAEMA) hyperbranched copolymers (HB) with hydrophobic MNPs and MNPs/curcumin mixtures. The hydrophobic species interact with the hydrophobic DIPAEMA segments of the polymeric assemblies. The formation and properties of the mixed nanostructures are investigated by utilization of dynamic light scattering (DLS) and cryogenic electron microscopy (cryo-TEM). Magnetophoresis studies were accomplished for the hybrid nanostructures of polymeric aggregates, before and after the encapsulation of curcumin, to explore their behavior upon the application of an external magnetic field, utilizing ultraviolet spectroscopy (UV-Vis). Afterwards, the colloidal stability of the hybrid MNPs/CUR-loaded nanostructures in the presence of serum and their fluorescence properties were studied. It was also demonstrated that the HB/MNP nanostructures can reduce pyrene concentration in aqueous solutions, thus paving ways for their utilization in water purification methodologies.

2. Materials and Methods

2.1. Materials

Tetrahydrofuran (THF, 99.9%, Sigma-Aldrich, Athens, Greece), curcumin was purchased from Merck (Athens, Greece), fetal bovine serum (FBS, Sigma-Aldrich, Athens, Greece). Synthesis of cobalt ferrite nanoparticles ($CoFe_2O_4$ NPs): hexane (Alfa Aesar, 99%, Haverhill, MA, USA), oleic acid (Penta, 97%, Prague, Czech Republic), ethanol absolute (Lach-ner, 99.8%, Neratovice, Czech Republic), 1-pentanol (Lach-ner, 99.8%, Neratovice, Czech Republic), 1-octanol (Sigma-Aldrich, 99%, Athens, Greece), sodium hydroxide (Penta, 97%, Prague, Czech Republic), iron (III) nitrate nonahydrate (Sigma-Aldrich, 98% Athens, Greece, cobalt (II) nitrate hexahydrate (Penta, 99%, Prague, Czech Republic).

2.2. Hyperbranched P(OEGMA-co-DIPAEMA) Copolymer Synthesis

The P(OEGMA-*co*-DIPAEMA) hyperbranched copolymers were synthesized by one-step Reversible Addition-Fragmentation Chain Transfer (RAFT) polymerization procedure utilizing ethylene glycol dimethacrylate (EGDMA) as the branching agent, 4-cyano-4(phenyl-carbonothioylthio) pentanoic acid (CPAD) as the chain transfer agent and 2,2′-azobis (isobutyronitrile), (AIBN) as the radical initiator. More details for the synthesis of hyperbranched copolymers are described in our previous work [33]. The molecular characteristics of all hyperbranched copolymers are presented in Table 1.

Table 1. Molecular characteristics of P(OEGMA-*co*-DIPAEMA) hyperbranched copolymers.

Sample	Mw [a] (g/mol) ($\times 10^4$)	Mw [b] (g/mol) ($\times 10^4$)	Mw/Mn [b]	%wt PDIPAEMA [c]	%wt POEGMA [c]
HB1	33.3	1.2	1.21	10	90
HB2	48.6	0.8	1.19	29	71
HB3	35.1	1.1	1.24	54	46

[a] Determined by static light scattering (SLS). [b] Determined by size exclusion chromatography (SEC). [c] Determined by nuclear magnetic resonance (^{1}H-NMR).

2.3. Synthesis of $CoFe_2O_4$ NPs

Hydrophobic $CoFe_2O_4$ nanoparticle dispersions were synthesized from corresponding iron and cobalt oleates under hydrothermal conditions [34]. Briefly, the metal oleates were prepared from iron and cobalt nitrates and sodium oleate solutions. These were mixed and refluxed with hexane, while the water phase was discarded afterwards. Hexane solvent was replaced by 1-pentanol and the desired amount of this mixture was placed into a Teflon lined steel autoclave (Berghof), together with 1-octanol and distilled water. Hydrothermal treatment took place in a preheated furnace at 180 °C for 10 h. The particles were further purified by centrifugation and redispersed in hexane. Stable hydrophobic dispersion was obtained thanks to the presence of the oleic acid layer attached to the cobalt ferrite particles. Oleic acid forms a uniform/non-separable structure with the magnetic core of the particles, stabilizes them and essentially contributes to the existence of positive/negative charge interactions with the hyperbranched polymer, which contains cationic segments.

2.4. Preparation of P(OEGMA-co-DIPAEMA) Magnetic Nanoparticles Hybrid Nanostructures

The process followed for the preparation of hybrid nanostructures is presented in detail as follows. Firstly, a weighed amount of amphiphilic hyperbranched copolymer P(OEGMA-*co*-DIPAEMA) (10 mg) was dissolved in THF (1 mL). Afterwards, an amount of a $CoFe_2O_4$ NPs dispersion in hexane was added to the solution. The desired concentration of $CoFe_2O_4$ in the mixture was set to 10–40%wt relative to the DIPAEMA content. Then the mixed solution was placed in a spherical flask and by using a rotary evaporator the organic solvents were evaporated (THF and Hexane), leaving a thin copolymer/MNPs mixed film on the flask walls. Thereafter, deionized water was added and gentle stirring resulted in the formation of hybrid nanostructures in aqueous media. The final copolymer concentration was 1×10^{-3} g mL^{-1}. In all cases no precipitate was observed for one month after preparation.

It is worth mentioning that it is generally known that in the case of electrostatic interaction of two oppositely charged components, the resulting aggregates have the same average composition as the stoichiometric composition utilized at the beginning. Some deviation from the average compositions should exist for each individual hybrid aggregate, but this is very difficult to determine.

2.5. Preparation of P(OEGMA-co-DIPAEMA) Magnetic Nanoparticle Hybrid Nanostructures Loaded with Curcumin

The solubilization protocol which was used to prepare the dual-multifunctional hybrid nanostructures is presented in detail in the following. Initially, a weighed amount of amphiphilic hyperbranched copolymer P(OEGMA-*co*-DIPAEMA) (10 mg) was dissolved in THF (1 mL). After, the proper amount of curcumin was dissolved in THF. A dispersion of MNPs in hexane was added to the solution. The concentration of MNPs in the mixture was 10 wt% and the concentration of curcumin was 20 wt% in respect to the DIPAEMA content. Afterwards, the mixed solution was placed in a spherical flask and solvents were evaporated using a rotary evaporator, resulting in a thin copolymer/MNPs/CUR mixed film on the flask walls. Thereafter, deionized water was added and gentle stirring resulted in the formation of hybrid nanostructures in aqueous media. The encapsulation of MNPs and CUR was performed only for HB2 and HB3 copolymers. Also, in case of MNPs/CUR-

loaded HB3 nanostructures the concentration of MNPs in the mixture was 40 wt% and the concentration of curcumin was 20 wt% according to the hydrophobic content of the copolymer. The final concentration of copolymer was 1×10^{-3} g/mL^{-1}. In all cases no precipitate was observed for one month.

2.6. Methods

Dynamic light scattering experiments were performed on an ALV/CGS-3 compact goniometer system (ALV Gmbh, Siemensstraße 4, 63225 Langen (Hessen, Germany)), equipped with a JDS Uniphase 22 mW He–Ne laser operating at 632.8 nm, connected to a digital ALV-5000/EPP multi-tau correlator with 288 channels and an ALV/LSE-5003 light scattering module for step-by-step control of the goniometer and control of the end position switch. The scattered light intensity measurements and acquisition of the correlation functions were performed five times and analyzed by the cumulants method and the CONTIN software. The latter provides the distributions of the apparent hydrodynamic radius (R_h), using the Laplace inverse transform of the correlation function by employing the Stokes–Einstein relationship. Measurements were carried out at 25 °C. The size data and figures presented below correspond to measurements at 90°. All solutions were filtered with a 0.45 μm hydrophilic PVDF filter prior to measurements.

Magnetophoresis experiments were performed utilizing a Perkin Elmer (Lambda 19) UV-Vis-NIR spectrophotometer (Waltham, MA, USA) by placing a cylindrical Nd-Fe-B magnet (dimensions: diameter = 20 mm, thickness = 10 mm, magnetization unit: N45, attraction/repulsion strength: max 16 kg) next to the cuvette holder. The wavelength for the measurements was chosen at 460 nm and the absorbance of the solutions containing the MNPs–loaded polymeric aggregates was recorded for 90 min under application of the magnet. It should be mentioned that the absorption at 460 nm is attributed to the presence of MNPS and not of the copolymer.

Also, for UV-Vis measurements on MNPs/pyrene-loaded copolymers the same instrument was utilized. As known from the literature, the prominent absorption bands of pyrene are at 320 nm [35]. The measurements were recorded after application of the magnet to the HB/MNPs solutions for 30 min.

Cryo-TEM images were obtained using a Tecnai F20 X TWIN microscope (FEI Company, Hillsboro, OR, USA) equipped with a field emission gun, operating at an acceleration voltage of 200 kV. Images were recorded on the Gatan Rio 16 CMOS 4 k camera (Gatan Inc., Pleasanton, CA, USA) and processed with Gatan Microscopy Suite (GMS) software (Gatan Inc., Pleasanton, CA, USA). Specimen preparation was done by vitrification of the aqueous solutions on grids with holey carbon film (Quantifoil R2/2; Quantifoil Micro Tools GmbH, Großlöbichau, Germany). Prior to use, the grids were activated for 15 s in oxygen plasma using a Femto plasma cleaner (Diener Electronic, Ebhausen, Germany). Cryo-samples were prepared by applying a droplet (3 μL) of the suspension to the grid, blotting with filter paper and immediate freezing in liquid ethane using a fully automated blotting device Vitrobot Mark IV (Thermo Fisher Scientific, Waltham, MA, USA). After preparation, the vitrified specimens were kept under liquid nitrogen until they were inserted into a cryo-TEM-holder Gatan 626 (Gatan Inc., Pleasanton, CA, USA) and analyzed in the TEM at −178 °C.

The X-ray diffraction (XRD) profiles were measured on a Bruker D8 Advance Twin diffractometer (Billerica, MA, USA) with a Cu tube (λ = 1.5418°A) and LYNXEYE_XE_T 1D detector. X-rays were generated under 40 kV and 40 mA tube operating condition. Scans were over the range of 20–70° 2θ with step size 0.1° and scan speed 5 s/step.

Fluorescence studies were accomplished in terms to specify the fluorescence properties of MNPs/CUR-loaded polymeric aggregates. The data were recorded with a NanoLog fluorometer (Horiba Jobin Yvon, Piscataway, NJ, USA), using a laser diode as the excitation source (Nano LED, 440 nm, 100 ps pulse width at 405 nm, and a UV TBX-PMT series detector (range 250–850 nm) from Horiba Jobin Yvon. Quartz cells of 1 cm path length were used, placing in them each time 1 mL of the solution to be measured.

Also, for fluorescence measurements on MNPs/pyrene-loaded copolymers the same instrument was utilized. Pyrene was used as a model hydrophobic agent and the I_1/I_3 ratio was measured after equilibration of the system. The concentration of pyrene was 3×10^{-6} M and that of the copolymer was 2×10^{-4} g/mL.

3. Results and Discussion

3.1. Characterization of $CoFe_2O_4$ NPs

DLS and XRD experiments to evaluate the size and the crystalline structure of the $CoFe_2O_4$ NPs are illustrated in the Supplementary Material in Figures S1 and S2 [36]. Also, Table S1 present the hydrodynamic radius (R_h) and size polydispersity index (PDI) of the $CoFe_2O_4$ NPs.

3.2. HB/MNP Hybrid Nanostructures

The self-organization of P(OEGMA-*co*-DIPAEMA) hyperbranched copolymers has been investigated extensively in our previous work [33]. In aqueous media, the hyperbranched copolymers form polymeric aggregates where the DIPAEMA component is forming the hydrophobic domains and OEGMA segments are constituting the hydrophilic corona. Induction of magnetic properties to the polymeric aggregates was accomplished by MNPs-stabilized with oleic acid which were interacting with the hydrophobic domains of the aggregates. The oleic acid-coated MNPs are miscible with the hydrophobic DIPAEMA domains; thus, the HB copolymer co-assembly with the MNPs was rather straightforward. Furthermore, both curcumin and MNPs were able to be entrapped simultaneously in the hydrophobic DIPAEMA domains in order to produce nanostructures with potential utilization in both imaging and therapy. OEGMA hydrophilic domains enhance solubility and stealth properties of the hybrid nanostructures. Table 2 presents the dynamic light scattering (DLS) results for all hybrid nanostructures prepared. In all cases, hybrid nanoparticles with sizes in the nanoscale, and relatively narrow size polydispersity were observed.

Table 2. DLS results for the P(OEGMA-co DIPAEMA) hyperbranched copolymers and MNPs-loaded nanostructures.

Sample	Hyperbranched Copolymer		HB/MNP Hybrid Nanostructures		
	R_h [a] (nm)	PDI [a]	MNPs %	R_h [a] (nm)	PDI [a]
HB1	3/97	0.5	10	152	0.23
			20	27/131 [b]	0.41
			30	32/105 [b]	0.29
HB2	4	0.5	10	165	0.27
			20	132	0.19
			30	142	0.3
HB3	11	0.39	10	27/120 [b]	0.5
			20	9/67 [b]	0.47
			30	12/67 [b]	0.44
			40	133	0.25

[a] Determined by dynamic light scattering (DLS) at 90°. [b] bimodal size distribution.

Based on the data in Table 2 it is observed that the co-assembly of MNPs with the hyperbranched copolymers was successful. It is worth noting that in the case of MNPs co-assembled with HB1 and HB2 copolymers, better defined structures were obtained, accompanied by relatively narrow size distributions, and exhibiting larger sizes after co-assembly. This observation should be related to the higher content of soluble OEGMA component which solvated and stabilized the nanostructures more effectively.

The encapsulation of MNPs in order to form the hybrid nanostructures was possible for all hyperbranched copolymers at the desired quantity mentioned above. DLS studies were performed, in order to explore the size of the MNPs-loaded polymeric aggregates (Table 1). Figure 1, represents a size distribution graph from CONTIN of the empty and MNPs-loaded nanoparticles, where the sizes appear to be affected after encapsulation of MNPs. In the case of HB1 copolymer containing 30 wt% MNPs a bimodal size distribution is observed, demonstrating the formation of two different populations of aggregates accompanied with relatively narrow size distributions for each type of aggregates. In the case of HB2 containing 30 wt% MNPs, hybrid polymeric co-assemblies with a relatively narrow size distribution are observed. The formed hybrid nanoassemblies exhibit larger sizes, in comparison to neat copolymer aggregates, depicting structural changes of the aggregates after co-assembly with MNPs. In the case of HB3 copolymer incorporating 30 wt% MNPs hybrid nanostructures with large sizes and a wider size distribution compared to neat copolymer aggregates are observed. The small size peak may represent neat polymeric nanoparticles or loaded-hybrid nanoparticles of small sizes. In contrast the HB3 based nanostructures containing the maximum level of MNPs (40 wt%) present much narrower and better-defined size distributions.

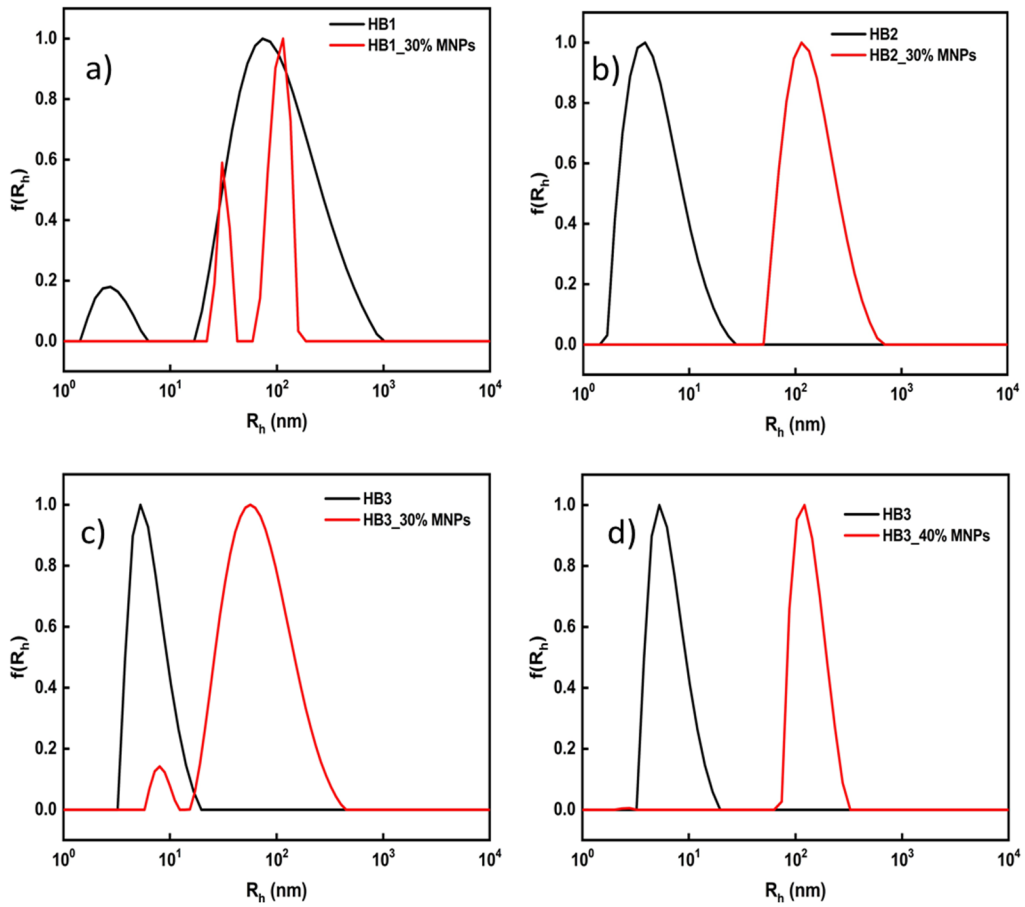

Figure 1. Comparative size distributions from DLS for hyperbranched copolymer nanostructures before and after co-assembly with MNPs. (**a**) HB1 vs. HB1/30% MNPs, (**b**) HB2 vs. HB2/30% MNPs, (**c**) HB3 vs. HB3/30% MNPs, (**d**) HB3 vs. HB3/40% MNPs.

Magnetophoresis studies were carried out in order to explore whether the MNPs included in the hybrid nanostructures retain the magnetic properties of the inorganic part after the co-assembly with the polymeric aggregates. The measurements were recorded for the HB3 hyperbranched copolymer containing the maximum contents of MNPs (30 and 40 wt% in respect to DIPAEMA component). Figure 2 illustrates that the HB3/MNPs hybrid nanostructures are accumulated in the side of the measuring cell closer to the magnet.

Moreover, in magnetophoresis studies performed with the aid of a UV-Vis instrument, it is clearly visible the decrease in the absorbance at 460 nm, because the inorganic part accumulates in the side where the magnet is placed. Figure 3 represents the magnetophoresis profiles, where for HB3/40 wt% MNPs it is observed that the MNPs-loaded aggregates have a powerful response when the external magnetic field is applied, presenting a significant reduction in the absorbance of the solution within the first 20 min, followed by a gradual and smaller decrease until the end of the measurement period. In contrast for the HB3 based nanostructures containing 30 wt% MNPs, no significant change in absorbance is observed. From the results obtained, it appears that MNPs are effectively entrapped at relatively high concentration in the polymeric aggregates and show response to the external magnetic stimulus applied.

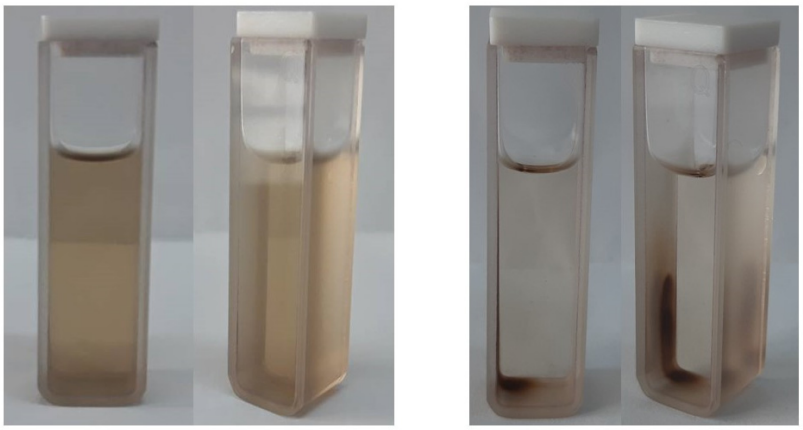

Figure 2. HB3/40% MNPs solution before (**left**) and after (**right**) the application of magnetic field.

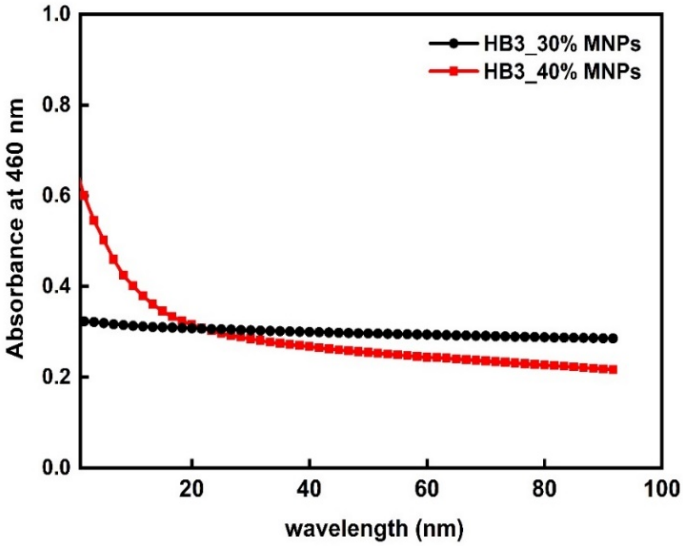

Figure 3. Characteristic magnetophoresis plot presenting absorbance as a function of time for MNPs-loaded nanostructures (HB3/MNP hybrid nanostructures at two different contents of MNPs).

3.3. Co-Encapsulation of MNPs and CUR Simultaneously into P(OEGMA-co-DIPAEMA) Polymeric Aggregates

The next step was to study if the polymeric aggregates could entrap both MNPs and a hydrophobic drug, such as curcumin, in the DIPAEMA domains forming dual loaded-multifunctional nanostructures. The process used for the preparation of P(OEGMA-*co*-DIPAEMA) aggregates loaded with MNPs and the anticancer drug curcumin was described above. The final concentration of the copolymers was 1×10^{-3} g/mL. The HB2 and HB3 hyperbranched copolymers were utilized for the double encapsulation, and character-

istic graphs of size distributions are presented in Figure 4. These copolymers presented a significant colloidal stability for more than 10 days after encapsulation of both MNPs and CUR. Regarding the HB1 copolymer, consisting mainly of the hydrophilic OEGMA component after mixing with MNPs, CUR precipitation occurred almost immediately. This fact can be attributed to the low content of hydrophobic DIPAEMA segments contained in this copolymer, leading to inefficient encapsulation of MNPs and CUR. The DLS technique was used to determine the size distributions of the MNPs/CUR-loaded nanoparticles (Table 3). In the cases of HB2/10% MNPs/20% CUR and HB3/10% MNPs/20% CUR fairly narrow size distributions were observed. This is more evident in the case of the HB2/10% MNPs/20% CUR assemblies where the size of hybrid nanostructures is shifted to larger dimensions. In the case of loaded HB3 copolymer the encapsulation of MNPs (10 wt%) and CUR results in a bimodal size distribution, where two sharp peaks appeared, specifying the two types of mixed nanoparticles present (with relatively narrow size distribution for each mixed nanoparticle population). In contrast, the addition of a higher amount of MNPs (40 wt%) led to the presence of one peak with wider size distribution, accompanied by a shift in dimensions to much larger sizes, demonstrating that at higher entrapment stoichiometries of MNPs the size distribution of hybrid nanostructures increases significantly. Both HB2 and HB3 hyperbranched copolymers seem to effectively encapsulate both MNPs and curcumin, forming well-defined nanostructures. This is also shown from the data presented in Table 3 demonstrating the successful encapsulation of both MNPs and CUR in the hyperbranched copolymers.

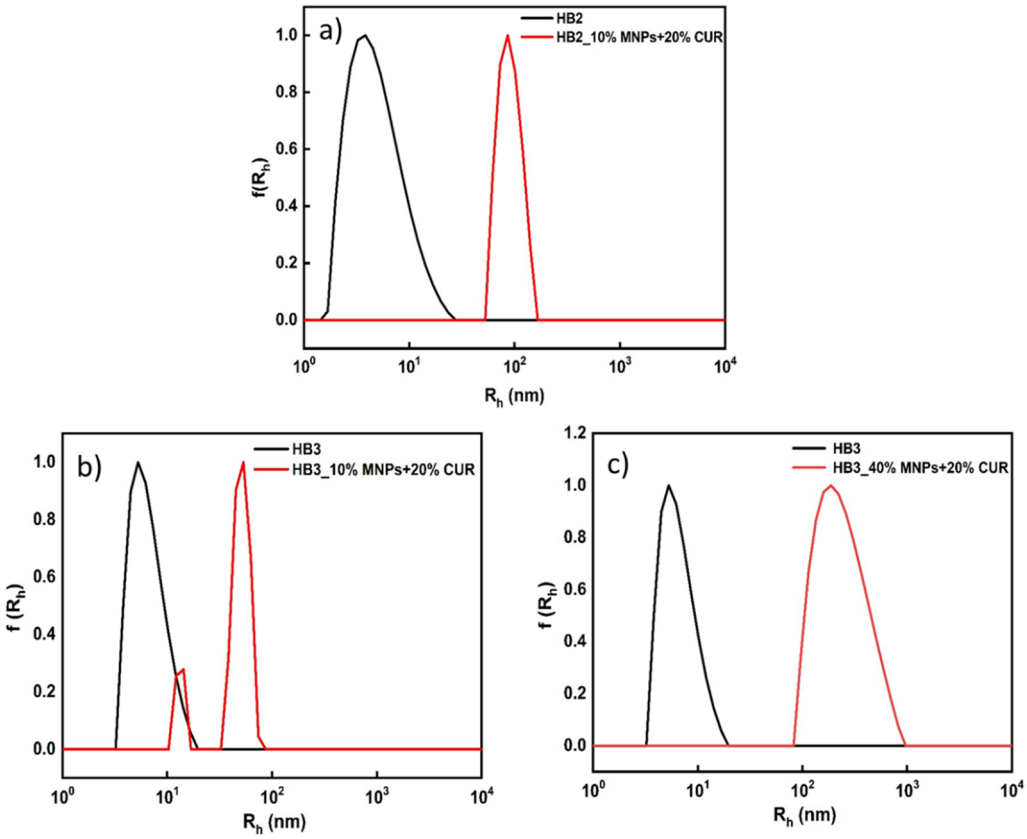

Figure 4. Comparative plots of size distributions from DLS measurements before and after simultaneous encapsulation of MNPs and CUR in HB2 and HB3 copolymers. (**a**) HB2 vs. HB2/10% MNPs + 20% CUR, (**b**) HB3 vs. HB3/10% MNPs + 20% CUR, (**c**) HB3 vs. HB3/40% MNPs + 20% CUR.

Table 3. DLS results for the MNPs/CUR-loaded nanostructures.

Sample	% MNPs	% CUR	R_h [a] (nm)	PDI [a]
HB2	10	20	89	0.26
HB3	10	20	13/51	0.36
	40	20	237	0.4

[a] Determined by DLS.

Based on the above results, the effective co-assembly of copolymer, MNPs and CUR is observed, which led to the formation of larger hybrid nanoparticles in the case of the higher loading level of MNPs and CUR (20 wt%).

Magnetophoresis studies were also carried out to explore whether three-component hybrid nanostructures containing the MNPs and CUR maintain some magnetic properties of the inorganic nanoparticles. The measurements were performed for the HB3 hyperbranched copolymer containing the maximum content of encapsulated MNPs (40 wt%). Figure 5 illustrates that the MNPs/CUR-loaded nanostructures are accumulated in the side of the measuring cell where the magnetic field is applied. Moreover, magnetophoresis studies performed using the UV-Vis instruments show the decrease of solution absorbance at 460 nm, again. Figure 6 presents the magnetophoresis graph, where it is observed that the MNPs/CUR-loaded aggregates have a significant response when an external magnetic field is applied. This is supported by the significant decrease in the absorbance of the solution within the first 20 min, followed by a gradual and smaller decrease until the end of the measurement. The acquired data are similar to those of the HB/MNPs-hybrid nanostructures, demonstrating that the encapsulation of CUR does not impart significant changes in the magnetic properties of the MNPs/CUR-loaded hyperbranched copolymer nanostructures, which maintain their ability to respond to an externally applied magnetic field.

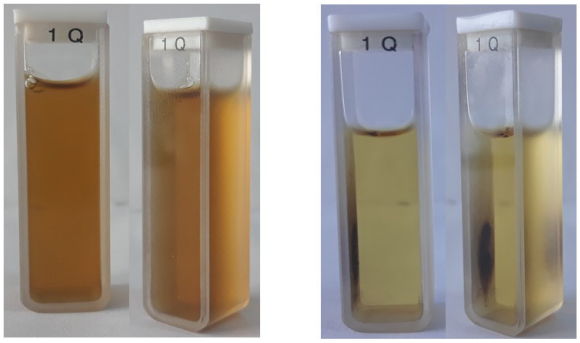

Figure 5. MNPs/CUR-loaded HB3 mixed solution before (**left**) and after (**right**) the application of magnetic field.

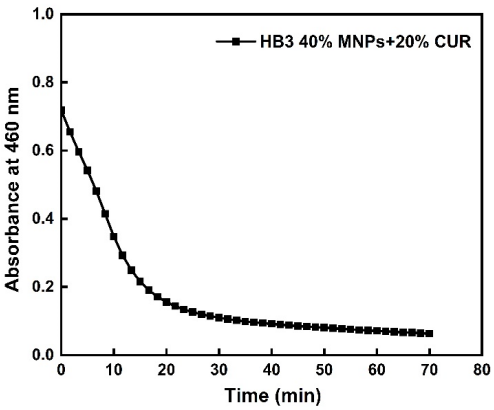

Figure 6. Characteristic magnetophoresis plot presenting absorbance as a function of time for MNPs/CUR-loaded HB3 hyperbranched copolymer nanostructures.

3.4. Cryo-TEM Imaging of the HB Based MNPs-Loaded and MNPS/CUR-Loaded Nanostructures

Cryo-TEM measurements presented a clearer picture of the morphology of the hybrid nanostructures prepared. The experiments were recorded at a copolymer concentration of 1×10^{-3} g/mL. In Figure 7, particles with strong contrast having a diameter 3–12 nm appear, corresponding to inorganic MNPs. These sizes are in agreement with DLS measurements where similar dimensions of MNPs (16 nm) were observed (Figure S1). After co-assembly of MNPs with the copolymer, mixed nanostructures are presented which have the form of irregular-shaped aggregates (Figure 7a). In Figure 7b it is observed that some of the magnetic particles form spherical structures with sizes of 50–70 nm, placed on the surface of the hyperbranched copolymer aggregates. It could be considered that MNPs decorate the surface of the copolymer assemblies. It should be taken into account that these are hyperbranched copolymers, which form aggregates with a diameter of ca. 20 nm, and their inner part is very dense due to the branching. Thus, the MNPs cannot penetrate but coat the surface of the copolymer assemblies. In conclusion, it appears that the structures observed by DLS and cryo-TEM are similar because the materials are in the same state during the measurement.

Additional information on the morphology of hybrid aggregates was obtained after the co-assembly of CUR and MNPs in hyperbranched copolymer aggregates. In particular, in Figure 9 no significant differences are observed in morphology and dimensions of the hybrid nanostructures after the entrapment of curcumin. This is in agreement with the DLS measurements, where the sizes were close to 100 nm. Particles form irregular-shaped aggregates again, and some of them form spherical structures with a size of 90–180 nm, probably MNPs are on the surface of spherical objects. Certainly, the main observation concerns the better self-assembly of the hybrid nanostructures, as shown by DLS, after the addition of CUR, resulting in better defined structures of hybrid nanoparticles.

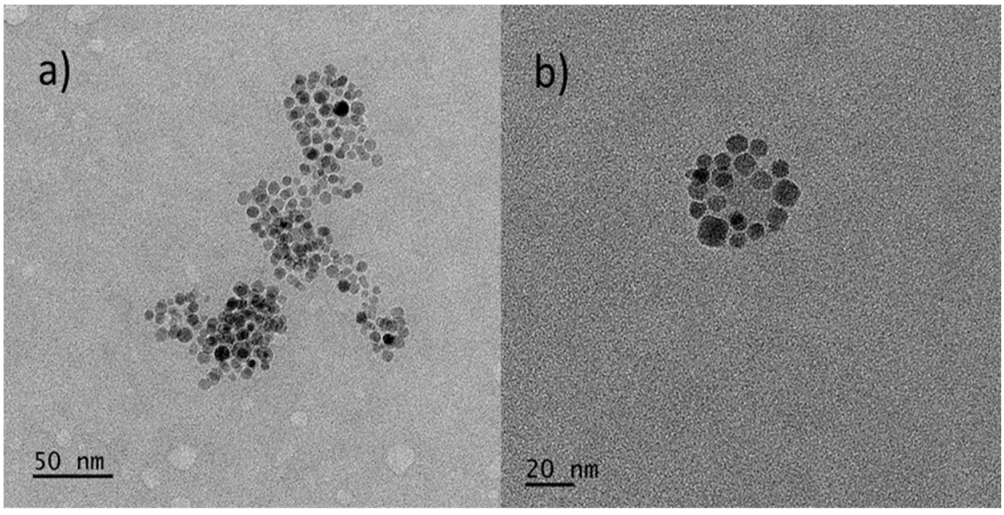

Figure 7. Cryo-TEM images for MNPs co-assembled with HB3 copolymer, depicting (**a**) cluster of aggregates and (**b**) isolated hybrid nanostructure.

Also, cryo-TEM images were recorded for the MNPs-loaded in the HB2 copolymer system, with 10 wt% MNPs. As shown in Figure 8, the MNPs have interacted with the polymer resulting in the formation of quite large aggregates which retain the same morphology as the mixed-aggregates of the HB3 copolymer. In particular, they appear to form spherical or irregular-shaped structures with a size of 40–300 nm, which corresponds to the dimensions from the DLS measurements. The DLS technique revealed the aggregation of the primary copolymer aggregates due to interaction with the MNPs. In particular, in Figure 8a hybrid nanostructures appear to have an MNPs-covered edge, created by MNPs decorating the surface of the particles. This morphology could be described as armored-like nanoparticles

or perhaps a raspberry-like structure [37–39]. Figure 8b shows some aggregated structures glued together forming larger objects.

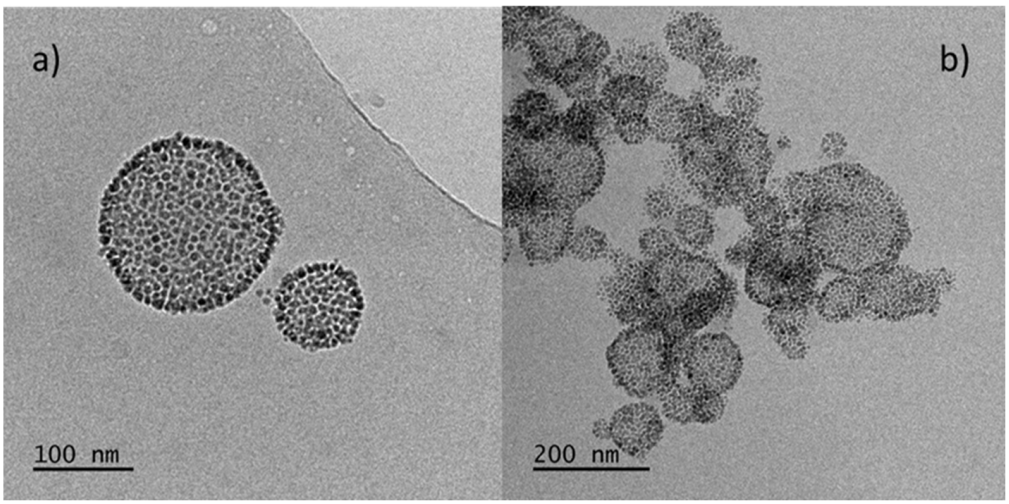

Figure 8. Cryo-TEM images for MNPs co-assembled with HB2 copolymer with 10 wt% MNPs content, (**a**) globular isolated co-assembled nanostructures (**b**) clusters of co-assembled nanostructures.

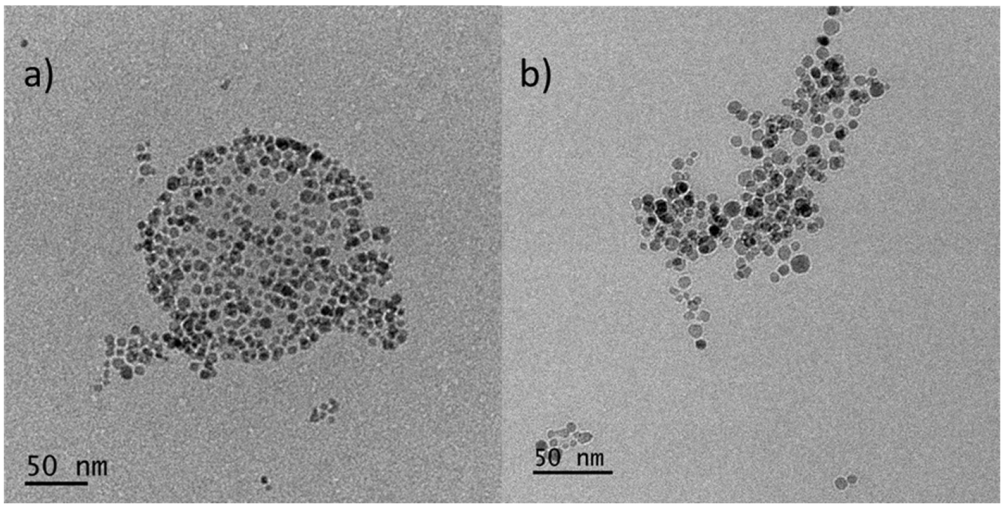

Figure 9. Cryo-TEM images for MNPs co-assemblies with HB2 copolymer with 10 wt% MNPs and 20 wt% CUR contents, depicting (**a**) large globular co-assembled nanostructures and (**b**) irregular co-assembled nanostructures.

3.5. Stability of the Hybrid Nanostructures in Biological Media and Their Fluorescence Properties

The subsequent studies on the hybrid nanostructures, was to investigate their colloidal stability under physiological conditions. This study was carried out by DLS. DLS measurements were recorded at 25 °C and at 90° angle after 3 h of mixing HB/MNPs/CUR hybrid nanostructures in the FBS/PBS mixed solution. Characteristic size distribution graphs are illustrated in Figure 10 for hybrid nanoparticles before and after mixing with FBS/PBS solution.

From the DLS results presented in Figure 10 for the MNPs/CUR containing nanostructures, it seems that their colloidal stability is not affected after addition of hybrid nanoparticles into FBS/PBS solutions. Specifically, the mixing of hybrid nanoparticles with FBS/PBS solution does not lead to any further aggregation of MNPS/CUR-loaded nanostructures and serum proteins in both FBS solutions (FBS/PBS 1:9 and 1:1). The data reveal the substantial stability of hybrid nanostructures under physiological conditions.

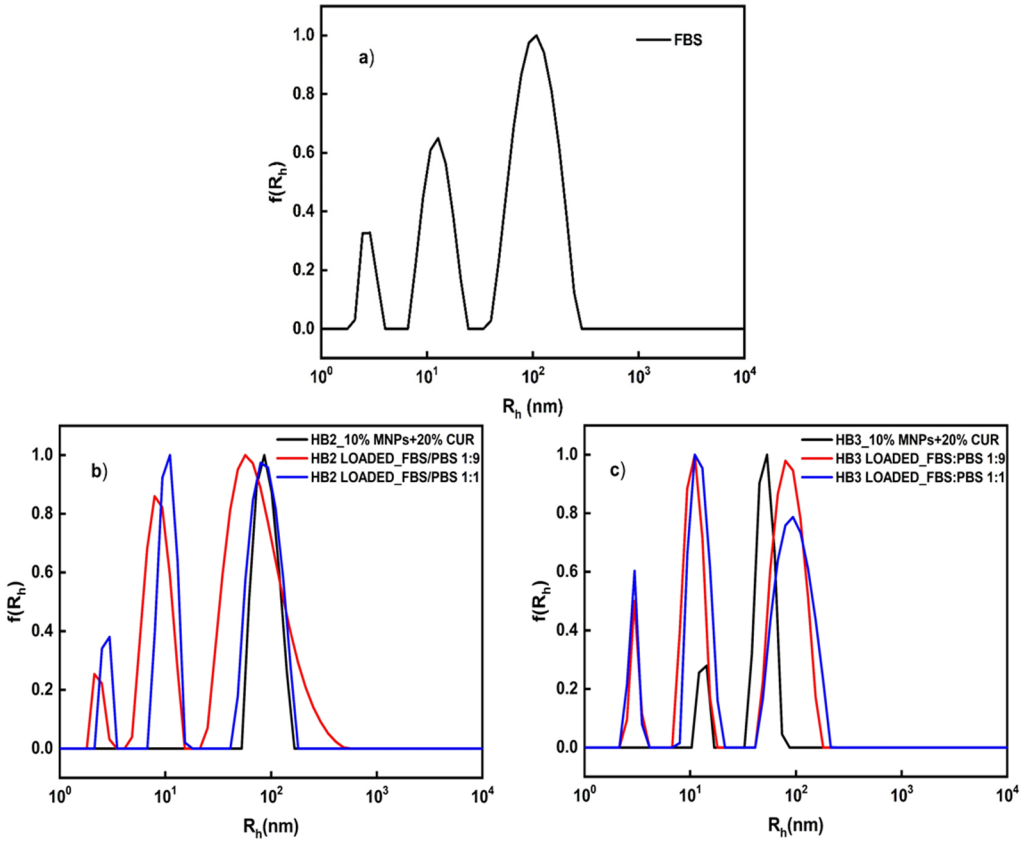

Figure 10. Comparative plots of size distributions from DLS measurements for: (**a**) FBS, (**b**) MNPs/CUR-loaded nanostructures before and after mixing with FBS:PBS (1:9), (**c**) MNPs/CUR-loaded nanostructures before and after mixing with FBS:PBS (1:1).

Next, the optical properties of encapsulated curcumin which provides strong endogenous fluorescence, a property that can be useful for bio-imaging applications [40,41], have been studied by fluorescence spectroscopy. It is worth noting that, in bio-imaging protocols, typically lower levels of active compounds are utilized compared to the present experiments. In our previous study we carried out an extensive fluorescence study of these hyperbranched copolymers containing CUR [33]. The results revealed significant fluorescence intensity at acidic and under physiological conditions. Therefore, in the present work we evaluated the three-component hybrid nanostructures based on the hyperbranched copolymers, MNPs and CUR. It is known from the literature that the miscibility of curcumin with water is very low (4.2 $\mu g/mL^{-1}$) [42,43]. Based on stoichiometric results, by CUR encapsulation in the HB/MNP nanostructures, its solubility does not increase. Actually, it occurs at lower levels (actual CUR concentrations for HB2/MNP 10% (Figure 11c) is 2 $\mu g/mL^{-1}$ and for HB3/MNP 10% (Figure 11d) is 2.9 $\mu g/mL^{-1}$). On the contrary, by encapsulation of 40 wt% MNPs and 20 wt% CUR in HB3 copolymer, curcumin solubility increases by 10 times (c_{CUR} = 41 $\mu g/mL^{-1}$) in comparison with the case of pure water. This phenomenon may be due to the fact that, in this particular case, the hybrid nanoparticles as revealed by DLS, form large aggregates resulting in the possibility of a higher rate of curcumin entrapment. Nevertheless, in all cases as shown in Figure 11, the formed nanostructures exhibit a remarkable fluorescence intensity. Specifically, the case of HB3 copolymer (Figure 11d) reveals a higher level of fluorescence intensity compared with the HB2 nanostructures (Figure 11c), most probably due to the higher quantity of encapsulated curcumin. Furthermore, as illustrated in Figure 8 the peak at 489 nm of curcumin in THF shifted to 505 nm, 514 nm, and 515 nm in aqueous solutions after the entrapment of MNPs and CUR. This displacement is presumably due to the hydrophobic interactions between both MNPs and CUR and the hydrophobic DIPAEMA component of

the copolymer. According to the results presented above the MNPs/CUR-loaded hybrid nanostructures may be utilized in bio-imaging application in addition to therapy.

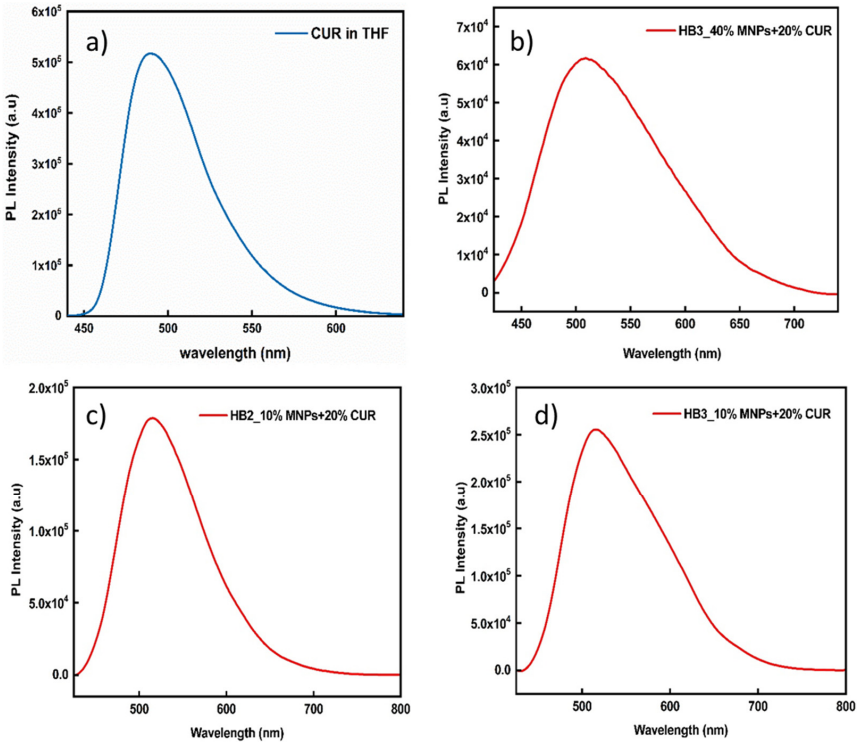

Figure 11. Fluorescence spectrum of (**a**) CUR in THF (c_{CUR} = 100 μg/mL^{-1}), (**b**) HB3/40% MNPs/CUR nanostructures, (**c**) HB2/10%MNPs/CUR nanostructures and (**d**) HB3/10% MNPs/CUR- nanostructures.

Another interesting application of these hybrid HB/MNP nanostructures in relation to water treatment technologies, and in particular removal of polycyclic hydrocarbon pollutants from aqueous reservoirs, is presented below in a semi-quantitative context. A pyrene solution (9 μL, 1 mM in acetone, final $c_{pyr} = 3 \times 10^{-6}$ M) was mixed with a HB3/40% MNP aqueous solution ($c_{pol} = 2 \times 10^{-4}$ g/mL). As shown in Figure 12 the absorption of pyrene aqueous solutions in the UV-Vis region, in conjunction with the pyrene spectrum by FS technique indicates, its encapsulation in the hydrophobic DIPAEMA part of the copolymer. Specifically, it appears that pyrene UV-Vis absorption decreases 3 times after the application of a magnetic field indicating that the HB/MNP adsorbs and removes part of the pyrene from the solution. The fluorescence spectrum obtained before the application of the magnetic field indicates the entrapment of the pyrene in the hydrophobic domains of the hybrid nanostructures, as the low value for the I_1/I_3 ratio indicates (Figure 12b).

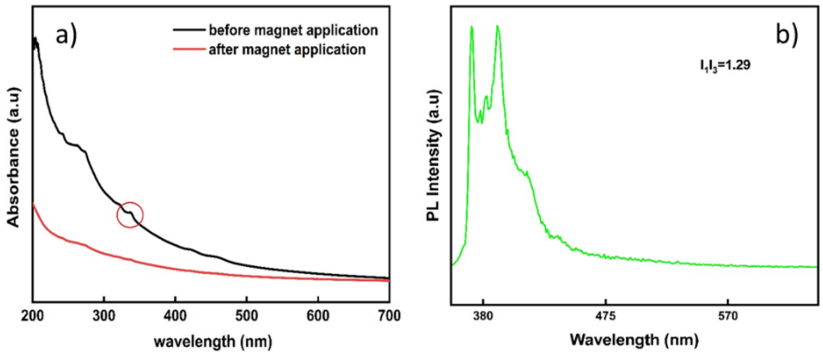

Figure 12. (**a**) UV-Vis spectrum of pyrene encapsulated in hybrid HB3/MNPs nanostructures and (**b**) FS spectrum of pyrene encapsulated in the hybrid nanostructures.

4. Conclusions

Multifunctional hybrid nanostructures formed by P(OEGMA-*co*-DIPAEMA) amphiphilic hyperbranched copolymers in aqueous media, were studied in detail. A plethora of physicochemical characterization techniques, such as DLS, UV-Vis, Cryo-TEM, and FS were utilized to investigate the properties of the acquired hybrid nanostructures. These hyperbranched copolymers self-organize in aggregates in aqueous media and were able to co-assemble with up to 40 wt% MNPs by interaction with the PDIPAEMA component, forming hybrid HB/MNP nanostructures. After co-assembly with MNPs, the sizes of the mixed aggregates are significantly increased, compared to the case of neat copolymer aggregates, where in the case of HB1 and HB2 mixed solution a rather narrower size distribution is observed, according to the DLS measurements. Magnetophoresis experiments revealed that the MNPs retain their magnetic properties after co-assembly with the copolymer aggregates.

Both CUR and MNPs were possible to be simultaneously encapsulated in the hyperbranched copolymer aggregates. Magnetophoresis measurements indicate that the HB/MNP/CUR three-component hybrid nanostructures present magnetic properties originating from the MNPs after encapsulation of CUR, leading to magnetically active mixed aggregates with the entrapped drug. DLS data revealed the outstanding colloidal stability of these hybrid nanosystems in the presence of serum proteins.

The mixed HB/MNP/CUR exhibit significant fluorescence and, thus, they may present potential for utilization in bio-imaging application. In summary, this work mainly presented the preparation of new hybrid nanostructures by co-assembly process and the characterization of their structure and properties. Our preliminary experiments could be useful for some potential applications of these hybrid nanostructures such as drug delivery, MRI imaging and even to remove aromatic pollutants from water. Of course, depending on the application fine tuning/choice of the materials utilized should be made based on properties like biocompatibility, temporal stability, and shelf-life of the structures among other considerations. This would require further experimentation which we hope it will be possible to perform in the future.

Supplementary Materials: The following supporting information can be downloaded at: https://www.mdpi.com/article/10.3390/nanomanufacturing2010004/s1, Table S1: DLS at 90° of the MNPs; Figure S1: Size distribution for the hydrophobic MNPs at 90°; Figure S2: XRD pattern of MNPs; Figure S3: Cryo-TEM images of the MNPs-loaded in HB3 copolymer with (a) 10 wt% MNPs and (b) 30 wt% MNPs; Figure S4: Cryo-TEM images of the MNPs-loaded in HB2 copolymer with (a) 10 wt% MNPs and (b) 30 wt% MNPs.

Author Contributions: Conceptualization, S.P.; methodology, S.P. and D.S.; formal analysis, D.S., A.F.; investigation, D.S., A.F.; resources, V.T., S.P., B.T.; data curation, D.S., A.F., A.A.; writing—original draft preparation, D.S., A.F.; writing—review and editing, D.S., A.F., B.T., A.A., V.T., S.P.; supervision, V.T., B.T., S.P.; project administration, S.P. All authors have read and agreed to the published version of the manuscript.

Funding: This research received no external funding.

Data Availability Statement: The data presented in this study are available on request from the corresponding author.

Conflicts of Interest: The authors declare no conflict of interest.

References

1. Arruebo, M.; Fernández-Pacheco, R.; Ibarra, M.R.; Santamaría, J. Magnetic nanoparticles for drug delivery. *Nano Today* **2007**, *2*, 22–32. [CrossRef]
2. Chroni, A.; Forys, A.; Trzebicka, B.; Alemayehu, A.; Tyrpekl, V.; Pispas, S. Poly [oligo (ethylene glycol) methacrylate]-b-poly [(vinyl benzyl trimethylammonium chloride)] Based Multifunctional Hybrid Nanostructures Encapsulating Magnetic Nanoparticles and DNA. *Polymers* **2020**, *12*, 1283. [CrossRef] [PubMed]
3. Indira, T.; Lakshmi, P. Magnetic nanoparticles—A review. *Int. J. Pharm. Sci. Nanotechnol.* **2010**, *3*, 1035–1042.
4. Krasia-Christoforou, T.; Georgiou, T.K. Polymeric theranostics: Using polymer-based systems for simultaneous imaging and therapy. *J. Mater. Chem. B* **2013**, *1*, 3002–3025. [CrossRef] [PubMed]

5. Namdeo, M.; Saxena, S.; Tankhiwale, R.; Bajpai, M.; Mohan, Y.Á.; Bajpai, S. Magnetic nanoparticles for drug delivery applications. *J. Nanosci. Nanotechnol.* **2008**, *8*, 3247–3271. [CrossRef] [PubMed]
6. Skandalis, A.; Sergides, A.; Bakandritsos, A.; Pispas, S. PLMA-b-POEGMA amphiphilic block copolymers as nanocarriers for the encapsulation of magnetic nanoparticles and indomethacin. *Polymers* **2018**, *10*, 14. [CrossRef]
7. Sun, C.; Lee, J.S.; Zhang, M. Magnetic nanoparticles in MR imaging and drug delivery. *Adv. Drug Deliv. Rev.* **2008**, *60*, 1252–1265. [CrossRef]
8. Ulbrich, K.; Hola, K.; Subr, V.; Bakandritsos, A.; Tucek, J.; Zboril, R. Targeted drug delivery with polymers and magnetic nanoparticles: Covalent and noncovalent approaches, release control, and clinical studies. *Chem. Rev.* **2016**, *116*, 5338–5431. [CrossRef]
9. Kafetzi, M.; Pispas, S.; Bao, X.; Yao, P. Amphiphilic QP (DMAEMA-*co*-LMA)-b-POEGMA Random-Block Terpolymers as Nanocarriers for Insulin. *Biomedicines* **2020**, *8*, 392. [CrossRef]
10. Liu, Y.; Fan, Y.; Yuan, Y.; Chen, Y.; Cheng, F.; Jiang, S.-C. Amphiphilic hyperbranched copolymers bearing a hyperbranched core and a dendritic shell as novel stabilizers rendering gold nanoparticles with an unprecedentedly long lifetime in the catalytic reduction of 4-nitrophenol. *J. Mater. Chem.* **2012**, *22*, 21173–21182. [CrossRef]
11. Luzon, M.; Boyer, C.; Peinado, C.; Corrales, T.; Whittaker, M.; Tao, L.; Davis, T.P. Water-soluble, thermoresponsive, hyperbranched copolymers based on PEG-methacrylates: Synthesis, characterization, and LCST behavior. *J. Polym. Sci. Part A Polym. Chem.* **2010**, *48*, 2783–2792. [CrossRef]
12. Pang, Y.; Liu, J.; Su, Y.; Zhu, B.; Huang, W.; Zhou, Y.; Zhu, X.; Yan, D. Bioreducible unimolecular micelles based on amphiphilic multiarm hyperbranched copolymers for triggered drug release. *Sci. China Chem.* **2010**, *53*, 2497–2508. [CrossRef]
13. Wang, D.; Chen, H.; Su, Y.; Qiu, F.; Zhu, L.; Huan, X.; Zhu, B.; Yan, D.; Guo, F.; Zhu, X. Supramolecular amphiphilic multiarm hyperbranched copolymer: Synthesis, self-assembly and drug delivery applications. *Polym. Chem.* **2013**, *4*, 85–94. [CrossRef]
14. Irfan, M.; Seiler, M. Encapsulation using hyperbranched polymers: From research and technologies to emerging applications. *Ind. Eng. Chem. Res.* **2010**, *49*, 1169–1196. [CrossRef]
15. Ma, C.; Qiu, S.; Yu, B.; Wang, J.; Wang, C.; Zeng, W.; Hu, Y. Economical and environment-friendly synthesis of a novel hyperbranched poly (aminomethylphosphine oxide-amine) as co-curing agent for simultaneous improvement of fire safety, glass transition temperature and toughness of epoxy resins. *Chem. Eng. J.* **2017**, *322*, 618–631. [CrossRef]
16. Chen, S.; Zhang, X.-Z.; Cheng, S.-X.; Zhuo, R.-X.; Gu, Z.-W. Functionalized amphiphilic hyperbranched polymers for targeted drug delivery. *Biomacromolecules* **2008**, *9*, 2578–2585. [CrossRef]
17. Deng, Y.; Saucier-Sawyer, J.K.; Hoimes, C.J.; Zhang, J.; Seo, Y.-E.; Andrejecsk, J.W.; Saltzman, W.M. The effect of hyperbranched polyglycerol coatings on drug delivery using degradable polymer nanoparticles. *Biomaterials* **2014**, *35*, 6595–6602. [CrossRef]
18. Jafari, M.; Abolmaali, S.S.; Najafi, H.; Tamaddon, A.M. Hyperbranched polyglycerol nanostructures for anti-biofouling, multi-functional drug delivery, bioimaging and theranostic applications. *Int. J. Pharm.* **2020**, *576*, 118959. [CrossRef]
19. Zhu, Q.; Qiu, F.; Zhu, B.; Zhu, X. Hyperbranched polymers for bioimaging. *RSC Adv.* **2013**, *3*, 2071–2083. [CrossRef]
20. Arkas, M.; Tsiourvas, D. Organic/inorganic hybrid nanospheres based on hyperbranched poly (ethylene imine) encapsulated into silica for the sorption of toxic metal ions and polycyclic aromatic hydrocarbons from water. *J. Hazard. Mater.* **2009**, *170*, 35–42. [CrossRef]
21. Harinath, Y.; Reddy, D.H.K.; Sharma, L.S.; Seshaiah, K. Development of hyperbranched polymer encapsulated magnetic adsorbent (Fe_3O_4@SiO_2–NH_2-PAA) and its application for decontamination of heavy metal ions. *J. Environ. Chem. Eng.* **2017**, *5*, 4994–5001. [CrossRef]
22. Tirotta, I.; Dichiarante, V.; Pigliacelli, C.; Cavallo, G.; Terraneo, G.; Bombelli, F.B.; Metrangolo, P.; Resnati, G. 19F magnetic resonance imaging (MRI): From design of materials to clinical applications. *Chem. Rev.* **2015**, *115*, 1106–1129. [CrossRef] [PubMed]
23. Wang, D.; Jin, Y.; Zhu, X.; Yan, D. Synthesis and applications of stimuli-responsive hyperbranched polymers. *Prog. Polym. Sci.* **2017**, *64*, 114–153. [CrossRef]
24. Ahmad, A.; Gupta, A.; Ansari, M.M.; Vyawahare, A.; Jayamurugan, G.; Khan, R. Hyperbranched polymer-functionalized magnetic nanoparticle-mediated hyperthermia and niclosamide bimodal therapy of colorectal cancer cells. *ACS Biomater. Sci. Eng.* **2019**, *6*, 1102–1111. [CrossRef]
25. Meikle, S.; Piñeiro, Y.; López, M.B.; Rivas, J.; Santin, M. Surface functionalization superparamagnetic nanoparticles conjugated with thermoresponsive poly (epsilon-lysine) dendrons tethered with carboxybetaine for the mild hyperthermia-controlled delivery of VEGF. *Acta Biomater.* **2016**, *40*, 235–242. [CrossRef]
26. Shi, Y.; Lei, G.; Li, Y.; Zhang, X.; Peng, R.; Hu, J.; Yuan, Z.; Liu, Y.; Shen, X.; Sun, N. In situ preparation of non-viral gene vectors with folate/magnetism dual targeting by hyperbranched polymers. *Eur. Polym. J.* **2020**, *127*, 109584. [CrossRef]
27. Laurent, S.; Forge, D.; Port, M.; Roch, A.; Robic, C.; Vander Elst, L.; Muller, R.N. Magnetic iron oxide nanoparticles: Synthesis, stabilization, vectorization, physicochemical characterizations, and biological applications. *Chem. Rev.* **2008**, *108*, 2064–2110. [CrossRef]
28. Zhang, L.; Gu, F.; Chan, J.; Wang, A.; Langer, R.; Farokhzad, O. Nanoparticles in medicine: Therapeutic applications and developments. *Clin. Pharmacol. Ther.* **2008**, *83*, 761–769. [CrossRef]
29. Arun, A.; Malrautu, P.; Laha, A.; Ramakrishna, S. Gelatin Nanofibers in Drug Delivery Systems and Tissue Engineering. *Eng. Sci.* **2021**, *16*, 71–81.

30. Hu, X.; Liu, G.; Li, Y.; Wang, X.; Liu, S. Cell-penetrating hyperbranched polyprodrug amphiphiles for synergistic reductive milieu-triggered drug release and enhanced magnetic resonance signals. *J. Am. Chem. Soc.* **2015**, *137*, 362–368. [CrossRef]
31. Zhao, C.; Han, Q.; Qin, H.; Yan, H.; Qian, Z.; Ma, Z.; Zhang, X.; Li, X. Biocompatible hyperbranched polyester magnetic nanocarrier for stimuli-responsive drug release. *J. Biomater. Sci. Polym. Ed.* **2017**, *28*, 616–628. [CrossRef] [PubMed]
32. Xie, W.; Shi, Y.; Wang, Y.; Zheng, Y.; Liu, H.; Hu, Q.; Wei, S.; Gu, H.; Guo, Z. Electrospun iron/cobalt alloy nanoparticles on carbon nanofibers towards exhaustive electrocatalytic degradation of tetracycline in wastewater. *Chem. Eng. J.* **2021**, *405*, 126585. [CrossRef]
33. Selianitis, D.; Pispas, S. Multi-responsive poly (oligo (ethylene glycol) methyl methacrylate)-*co*-poly (2-(diisopropylamino) ethyl methacrylate) hyperbranched copolymers via reversible addition fragmentation chain transfer polymerization. *Polym. Chem.* **2021**, *12*, 6582–6593. [CrossRef]
34. Repko, A.; Vejpravová, J.; Vacková, T.; Zákutná, D.; Nižňanský, D. Oleate-based hydrothermal preparation of $CoFe_2O_4$ nanoparticles, and their magnetic properties with respect to particle size and surface coating. *J. Magn. Magn. Mater.* **2015**, *390*, 142–151. [CrossRef]
35. Gališinová, J.; Andriamainty, F.; Malík, I.; Čižmárik, J.; Karlovska, J.; Sichrovska, L. A Study of Local Anaesthetics. Part 202. Determination of the Critical Micellar Concentration of Carbisocainium Chloride in Water Using Spectral Methods and the Probe Pyrene. *Eur. Pharm. J.* **2013**, *60*, 1–6. [CrossRef]
36. Zhao, S.; Ma, D.; Jin, W. Preparation of $CoFe_2O_4$ Nanocrystallites by Solvothermal Process and Its Catalytic Activity on the Thermal Decomposition of Ammonium Perchlorate. *J. Nanomater.* **2010**, *2010*, 842816. [CrossRef]
37. Fang, S.; Tong, Z.; Nie, P.; Liu, G.; Zhang, X. Raspberry-like nanostructured silicon composite anode for high-performance lithium-ion batteries. *ACS Appl. Mater. Interfaces* **2017**, *9*, 18766–18773. [CrossRef]
38. Mai, Y.; Eisenberg, A. Selective localization of preformed nanoparticles in morphologically controllable block copolymer aggregates in solution. *Acc. Chem. Res.* **2012**, *45*, 1657–1666. [CrossRef]
39. Kim, M.P.; Yi, G.-R. Nanostructured colloidal particles by confined self-assembly of block copolymers in evaporative droplets. *Front. Mater.* **2015**, *2*, 45. [CrossRef]
40. Selianitis, D.; Pispas, S. P (MMA-*co*-HPMA)-b-POEGMA copolymers: Synthesis, micelle formation in aqueous media and drug encapsulation. *Polym. Int.* **2021**, *70*, 1508–1522. [CrossRef]
41. Skandalis, A.; Selianitis, D.; Pispas, S. PnBA-b-PNIPAM-b-PDMAEA Thermo-Responsive Triblock Terpolymers and Their Quaternized Analogs as Gene and Drug Delivery Vectors. *Polymers* **2021**, *13*, 2361. [CrossRef] [PubMed]
42. Liu, M.; Teng, C.P.; Win, K.Y.; Chen, Y.; Zhang, X.; Yang, D.P.; Li, Z.; Ye, E. Polymeric encapsulation of turmeric extract for bioimaging and antimicrobial applications. *Macromol. Rapid Commun.* **2019**, *40*, 1800216. [CrossRef] [PubMed]
43. Nguyen, H.N.; Ha, P.T.; Sao Nguyen, A.; Nguyen, D.T.; Do, H.D.; Thi, Q.N.; Thi, M.N.H. Curcumin as fluorescent probe for directly monitoring in vitro uptake of curcumin combined paclitaxel loaded PLA-TPGS nanoparticles. *Adv. Nat. Sci. Nanosci. Nanotechnol.* **2016**, *7*, 025001. [CrossRef]